10-13-2017

Measuring Long-Range 13C–13C Correlations on a Surface under Natural Abundance Using Dynamic Nuclear Polarization-Enhanced Solid-State Nuclear Magnetic Resonance

Takeshi Kobayashi
Ames Laboratory, tkobayashi@ameslab.gov

Igor I. Slowing
Iowa State University and Ames Laboratory, islowing@iastate.edu

Marek Pruski
Iowa State University and Ames Laboratory, mpruski@iastate.edu

Measuring Long-Range 13C–13C Correlations on a Surface under Natural Abundance Using Dynamic Nuclear Polarization-Enhanced Solid-State Nuclear Magnetic Resonance

Abstract
We report that spatial (<1>nm) proximity between different molecules in solid bulk materials and, for the first time, different moieties on the surface of a catalyst, can be established without isotope enrichment by means of homonuclear CHHC solid-state nuclear magnetic resonance experiment. This 13C–13C correlation measurement, which hitherto was not possible for natural-abundance solids, was enabled by the use of dynamic nuclear polarization. Importantly, it allows the study of long-range correlations in a variety of materials with high resolution.

Keywords
Dynamic Nuclear Polarization, Solid-state NMR, homonuclear correlation, natural abundance, catalyst surface

Disciplines
Chemistry | Materials Chemistry | Physical Chemistry

Measuring Long Range ^{13}C-^{13}C Correlations on Surface under Natural Abundance Using DNP-enhanced Solid-state NMR

Takeshi Kobayashi,[a] *Igor, Slowing,*[a,b] *and Marek, Pruski*[a,b,]*

Ames Laboratory, U.S. Department of Energy, Ames, Iowa, 50010, United States

Department of Chemistry, Iowa State University, Ames, Iowa, 50010, United States.

*Corresponding Author

mpruski@iastate.edu

Abstract

We report that spatial (<1 nm) proximity between different molecules in solid bulk materials and, for the first time, different moieties on the surface of a catalyst, can be established without isotope enrichment by means of homonuclear CHHC solid-state (SS)NMR experiment. This ^{13}C-^{13}C correlation measurement, which hitherto was not possible to natural-abundance solids, was enabled by the use of dynamic nuclear polarization (DNP). Importantly, it allows the study of long-range correlations in a variety of materials with high-resolution.

KEYWORDS

Dynamic Nuclear Polarization; Solid-state NMR; homonuclear correlation; natural abundance; catalyst surface

1. Introduction

One of the long-standing challenges in the studies of complex materials by SSNMR spectroscopy is the determination of *intermolecular* order, e.g. to elucidate the structure of blended materials, host-guest pairs, or cooperative catalysts. This challenge can be partly addressed by the acquisition of highly sensitive two-dimensional (2D) ^{1}H-^{1}H correlation NMR spectra. Indeed, elegant examples of such spectra can be found in the literature, however low resolution and narrow chemical shift range necessitate the use of ultrafast magic angle spinning (MAS) and/or ^{1}H homonuclear decoupling and limit their applications to simple molecular systems.[1-2] Heteronuclear ^{1}H-X spectroscopy can be applied to take advantage of the wider chemical shift range of heteronuclei (such as ^{13}C and ^{15}N), but the low efficiency of long-range polarization transfers, and dipolar truncation effects, strongly favor *intramolecular* ^{1}H-X correlations.[2] In addition, heteronuclei typically possess lower gyromagnetic ratio γ and natural abundance (NA), which challenges SSNMR's already low sensitivity. These shortcomings are further exemplified in X-X homonuclear correlation experiments, which can, in theory, offer the highest resolution, but have been until recently prohibitively insensitive under natural abundance. This is the case since the probability of finding an interacting pair of nuclei depends on the square of their NA. As a result, historically, homonuclear correlation experiments between heteronuclei required isotopic enrichment, which is often nontrivial, always expensive, and leads to an unwanted effect referred to as dipolar truncation.

Recent advances in dynamic nuclear polarization (DNP) SSNMR,[3] such as the development of gyrotrons,[4] low-temperature MAS probes,[5] and biradical polarizing agents,[6,7] have offered unprecedented signal enhancements and created opportunities for homonuclear double-quantum-single-quantum (DQ/SQ) correlation spectroscopy between unreceptive and rare nuclei, such as

^{13}C and ^{29}Si in natural-abundance solids.[8-17] In particular, DNP facilitated the acquisition of high-quality homonuclear ^{13}C-^{13}C correlation spectra in a practical experimental time.[8-10, 12-15] Note that such measurements were unimaginable using conventional NMR since the NA of ^{13}C is only 1.1 %. The first ^{13}C-^{13}C spectra were acquired by Rossini et al. on glucose and sulfathiazole,[9] using DQ/SQ with POST-C7[18] dipolar recoupling scheme as well as scalar recoupling via INADEQUATE,[19] and by Takahashi et al. on microcrystalline cellulose, who used the DQ/SQ-POST-C7 scheme.[8] Most recently, these techniques were applied to reveal the molecular conformations and crystal packing in pharmaceuticals (theophylline),[12] determine *de novo* structure of nucleoside (deoxyguanosine),[13] study the catalytic decomposition of biomass[14] and probe non-covalent π-stacking interactions responsible for the self-assembly of peptides into nanotubes.[15] The fact that such measurements can now be performed under NA offers an additional benefit of suppressing the dipolar truncation, thereby allowing long-range polarization transfers and accurate measurements of ^{13}C-^{13}C distances of up to 0.7 nm, which is remarkable given the inverse-cubed dependence of the dipolar coupling on the internuclear spacing.[12, 15]

The advantage of DQ/SQ over single-quantum correlation (SQ/SQ) approach[20] is that the DQ filtering silences the unwanted diagonal resonances from the uncorrelated magnetization which pollute the SQ/SQ-type spectra. The shortcoming of DQ/SQ lies in susceptibility to relaxation-induced losses during long dipolar or *J*-based recoupling periods, which indeed impeded our efforts to use this technique to measure long-range intermolecular order on surfaces. The traditional SQ/SQ ^{13}C-^{13}C 'spin-diffusion' approach, however, also proved inefficient owing to the small dipolar ^{13}C-^{13}C interactions and the energy mismatch under fast MAS due to large variation of chemical shifts. To enhance such polarization transfer, a variety of radio-frequency (RF)-driven recoupling sequences, for example DARR,[21] RAD[22] and PARIS,[23] have been

proposed. While these so-called proton-driven spin diffusion techniques facilitate a more efficient recoupling of spectrally distant resonances, their spatial range remains limited by the weak dipolar coupling between heteronuclei, which is exacerbated at NA; note, for example, that the ^{13}C-^{13}C dipolar coupling drops below 100 Hz at $r_{C\text{-}C} \cong 0.42$ nm.

A possible way to alleviate these shortcomings is to use an SQ/SQ scheme proposed by Spiess et al.,[24] in which X-edited ^{1}H polarization is transported by ^{1}H-^{1}H spin diffusion during a longitudinal mixing period placed between two cross-polarization transfers. This technique, and its derivative pulse sequences, known as CP^3 or XHHX (Figure 1),[25-28] were successfully used to detect long-range ^{13}C-^{13}C correlations and provided useful structural information in isotopically labelled polymers and biological materials. Here, we demonstrate that this ^{1}H-mediated homonuclear correlation scheme can be boosted by the use of DNP (Figure 1) to enable, for the first time, long-range correlation spectroscopy on the surface at natural isotopic abundance.

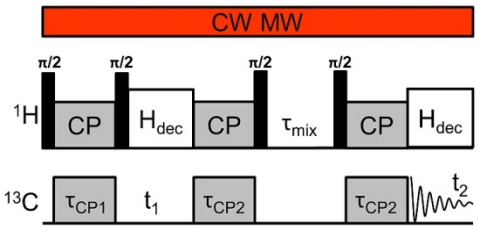

Figure 1. Schematic diagram of the pulse sequence used in this study in conjunction with continuous-wave microwave (CW MW) irradiation. Pulse sequence and phase cycling follow those reported in reference 25.

2. Experimental

2.1. Synthesis of functionalized mesoporous silica nanoparticles (MSNs). A bi-functional material was prepared via co-condensation method as follows. A mixture of cetyltrimethylammonium bromide (CTAB, $CH_3(CH_2)_{15}N(CH_3)_3Br$) (1.0 g), sodium hydroxide (3.5 mL, 2.0 M), and water (480 mL) was heated to 80°C in flask with constant stirring. After

one hour, 5 mL of tetraethylorthosilicate (TEOS) was added drop-wise for the duration of 5 minutes. Immediately after the TEOS addition, 0.5 mL of (3-mercaptopropyl) trimethoxysilane and 0.5 mL of phenyltrimethoxysilane were added to the system. After heating at 80 °C for 2 hours, the solution was filtered, washed with abundant water and then with abundant methanol, and the resulting white solid was vacuum-dried overnight. The surfactant was then removed by refluxing the dry solid in a solution of 0.5 mL of 2.0 M hydrochloric acid and 50 mL of methanol for 6 hours at 60 °C. The surfactant-removed sample was then filtered, washed with abundant methanol and dried in a Schlenk line at 100 °C under vacuum overnight.

The loadings of mercaptopropyl (MP) and phenyl (Ph) groups were estimated by spin counting using a ^{1}H DPMAS NMR measurement. Prior to the ^{1}H NMR experiments, the sample was thoroughly deuterated to avoid interference of hydroxyl proton signals as follows. The Ph/MP-MSN was suspended in D_2O (99.9 atom %) with stirring at room temperature overnight, after which the supernatant was decanted. After repeating the process three times, each time with fresh D_2O, the Ph/MP-MSN was dehydrated at 100 °C under vacuum. The ^{1}H spin counting, with respect to the ^{1}H NMR spectrum of known amount of hexamethylbenzene, determined the loadings of MP and Ph groups to be 2.1 mmol/g and 1.7 mmol/g, respectively.

2.2. DNP-enhanced solid-state NMR experiments. The DNP-enhanced measurements were performed using a Bruker Biospin AVANCE III 400 DNP NMR spectrometer, equipped with a 264 GHz gyrotron and a low-temperature (~115 K) MAS probe. The samples were exposed to radical solutions by incipient wetness impregnation in a mortar and then packed into 3.2-mm sapphire MAS rotors. Experimental details for the DNP-enhanced NMR experiments are given in figure captions, using the following symbols: ν_R denotes the magic angle spinning rate; τ_{CP}, the cross-polarization time; τ_{mix}, the mixing time; Δt_1, the increment of t_1 during 2D acquisition;

τ_{RD}, the recycle delay and AT, the total acquisition time. The ^{13}C chemical shifts are referenced to TMS at 0 ppm.

3. Results and Discussion

We first acquired 2D ^{13}C-^{13}C correlations for a polyacrylamide polymer using both the CHHC and the DARR scheme. The sample was impregnated with a 10 mM H_2O/D_2O (10/90 v/v) solution of the AMUPol biradical[6] and spun at ν_R = 10 kHz at a temperature of 115 K. As can be seen in Figure 2b, the CHHC spectrum acquired with τ_{mix} = 50 μs exhibited only one-bond correlations (C1-C2 and C2-C3, indicated by solid lines) with strong signal intensity, and a weak two-bond correlation (C1-C3, a dotted line). The C1-C3 cross-peak was noticeably stronger in the spectrum acquired with τ_{mix} = 100 μs (Figure 2c). However, no off-diagonal peaks were observed by DARR for polyacrylamide using the same number of scans, regardless of the mixing time (we tested 20 ms ≤ τ_{mix} ≤ 200 ms; the spectrum for τ_{mix} = 100 ms is shown in Figure S1 in Supporting Information). Clearly, the ^{1}H-^{1}H spin diffusion played an important role in mediating the propagation of ^{13}C magnetization in the sample.

An important quality of the natural-abundance CHHC method is the relatively low intensity of diagonal peaks, which in spectra taken with appropriate mixing time show comparable height to the off-diagonal signals (Figure 2d). As a result, the C2-C3 correlation signals observed by the CHHC scheme were well resolved from the diagonal signals (Figure 2b and c, insets), despite the resonance frequencies of C2 and C3 being separated by only ~5 ppm. The suppression of diagonal signals in CHHC spectra of NA samples is due to the large ^{1}H spin bath, which here also includes the solvent and thoroughly depolarizes the rare spins during the second cross-polarization. This is in stark contrast to the DNP-enhanced ^{13}C-^{13}C homonuclear correlation

spectra of cellulose obtained by the DARR recoupling, where more than 90-fold ratio between the intensities of diagonal and non-diagolnal peaks was reported.[8]

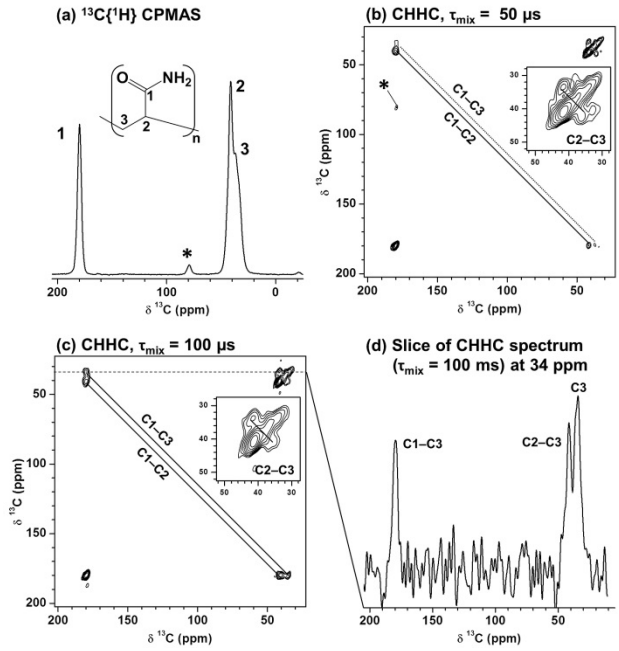

Figure 2. DNP-enhanced 1D $^{13}C\{^1H\}$ CPMAS (a) and 2D ^{13}C-^{13}C homonuclear correlation spectra for naturally abundant polyacrylamide obtained using the CHHC scheme with τ_{mix} = 50 μs (b) and 100 μs (c), slice of spectrum c at 34 ppm along F2 axis (d). The 1D CPMAS spectrum was acquired with ν_R = 10 kHz, using τ_{CP} = 4 ms, τ_{RD} = 6 s, and 4 scans. The CHHC spectra were obtained with ν_R = 10 kHz, using τ_{CP1} = 4 ms, τ_{CP2} = 1 ms, 32 t_1 steps with Δt_1 = 50 μs, τ_{RD} = 6 s, 32 scans per row, and AT = 3.5 h. The asterisk in (a and b) marks a spinning sideband.

The CHHC scheme was then applied to a semicrystalline cellulose sample, in this case impregnated with a 10 mM H_2O solution of the AMUPol radical. With τ_{mix} = 200 μs, three sets of correlation signals were observed (Figure 3b), assigned to C2,5-C6, C3-C2,C5 and C1-C2,C5 carbon pairs. Note that the C2 and C5 signals overlap, and that the last two pairs of cross-peaks are dominated by one-bond correlations, C3-C2 and C1-C2. When the mixing time was increased to 500 μs (Figure 3c), the spectrum showed not only one- and two-bond correlations but also three-bond C3–C6 correlation that was not observed by the DQ recoupling scheme.[8] The

remaining one- (C4-C3), two-(C4-C6) and three-bond (C1-C6) correlations finally appeared after τ_{mix} = 1 ms. In crystalline cellulose, which consists of a stacks of linear chains of β(1→4) glucose monomers, the intra-monomer C1-C6 and C3-C6 distances (0.37 nm and 0.39 nm, respectively) are very close to the corresponding inter-monomer distances (0.39 nm and 0.40 nm, respectively).[29] Thus, the observed long-range off-diagonal signals most likely result from both intra- and inter-unit, as well as inter-chain correlations. The three-bond C2-C5 (0.29 nm) and four-bond C2-C6 (0.42 nm) correlations were not resolved due to the superposition of C2 and C5 signals.

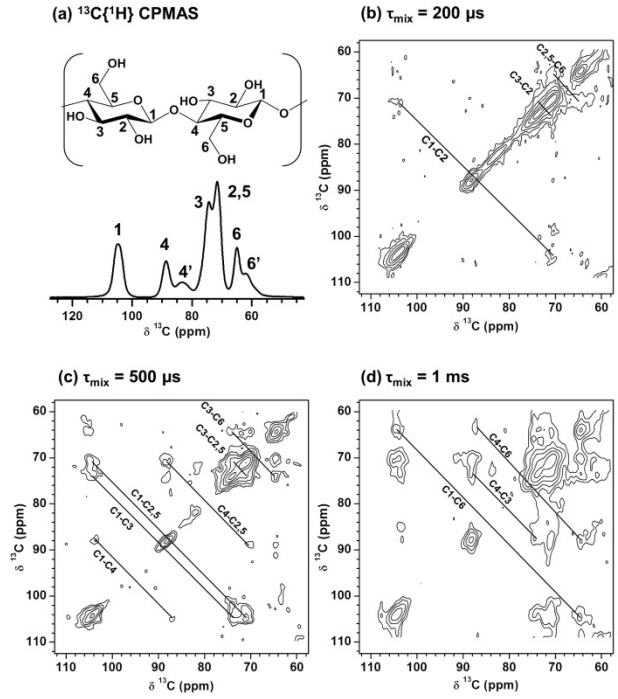

Figure 3. DNP-enhanced 1D $^{13}C\{^1H\}$ CPMAS (a), 2D ^{13}C-^{13}C homonuclear correlation spectra of naturally abundant semicrystalline cellulose obtained using the CHHC scheme with τ_{mix} = 200 µs (b), 500 µs (c) and 1 ms (d). The DNP-enhanced 1D $^{13}C\{^1H\}$ CPMAS spectrum (a) was obtained with ν_R = 10 kHz, τ_{CP} = 2 ms, and 4 scans. The 2D CHHC spectra (b-d) were obtained with ν_R = 10 kHz, τ_{CP} = 2 ms, τ_{CP2} = 500 µs, 32 t_1 steps with Δt_1 = 200 µs, 32 scans per row, τ_{RD} = 6 s, and AT = 3.4 h. Signals 4' and 6' represent C4 and C6 in the amorphous phase.

The spatial range of correlations detectable by the CHHC scheme is determined by the spin diffusion rate of the ^{13}C-edited ^{1}H longitudinal magnetization. The root-mean-square displacement of 3D spin diffusion is given by $\langle r(t) \rangle = \sqrt{6Dt}$, where t and D represent time and the diffusion coefficient, respectively. Assuming the ^{1}H diffusion coefficient to be on the order of 2 x 10^2 nm^2/s, as was measured in rigid polymers by "NMR hole burning" under slow MAS (2.4 kHz),[30] the ^{1}H spin diffusion is expected to propagate within a radius of approximately 0.5 nm from its origin during τ_{mix} = 200 μs. In addition, ^{1}H magnetization can diffuse during the CP periods, albeit at a scaled diffusion rate,[30] as we indeed determined by measuring a series of ^{13}C-^{13}C spectra as a function of τ_{CP2} with τ_{mix} = 0 (see Figure S2 in Supporting Information). The fact that only some of the one-bond correlations, C1-C2 and C3-C2, appeared in the spectra after τ_{mix} = 200 μs (Figure 3b), may be attributed to the faster MAS rate used in our study (10 kHz), and the orientational dependence of ^{1}H spin diffusion, suggested by the fact that the build-up rates of correlation signals of similarly separated pairs did not coincide. This anisotropy is not surprising because the spatial distribution of ^{1}H nuclei in cellulose is inhomogeneous. We finally note that an increase of τ_{mix} beyond 1 ms resulted in a significant loss of both diagonal and off-diagonal signals in the spectra (not shown), which can be attributed to dissipation of ^{1}H magnetization from cellulose into the frozen solvent. As is the case in the polyacrylamide, the diagonal and off-diagonal peaks in the cellulose sample were comparable (Figure S3 in Supporting Information), which enabled to resolve closely spaced off-diagonal signals attributed to the C3-C2,5 correlations (here by just 2 ppm) from the diagonal signals (see Figure 3c).

We finally examined the proximity of two different organic functional groups, phenyl (Ph) and mercaptopropyl (MP), covalently co-attached onto the mesoporous silica surface. The sample was impregnated with a 16 mM solution of the TekPol[7] biradical in 98%-deuterated 1,1,2,2-

tetrachloroethane (TCE). Taking into account the loadings of functional groups (2.1 mmol/g and 1.7 mmol/g for MP and Ph, respectively) and assuming the surface area of ~800 m^2/g, which is typical for functionalized mesoporous silica, the average intermolecular distance is estimated to be ~0.65 nm (with the density of organic groups being ~2.9 nm^{-2}). The cross peaks in the spectra with τ_{mix} = 100 μs (Figure 4b) represent Ph-Ph and MP-MP correlations, which are most likely due to intramolecular interactions. When the τ_{mix} was extended to 200 μs, remarkably the DNP-enhanced CHHC scheme could detect intermolecular Ph-MP correlations of surface species at natural abundance (Figure 4c), establishing for the first time the proximity of different functional groups on the silica surface on the nm scale. This development is particularly significant for the design of cooperative heterogeneous catalysts.

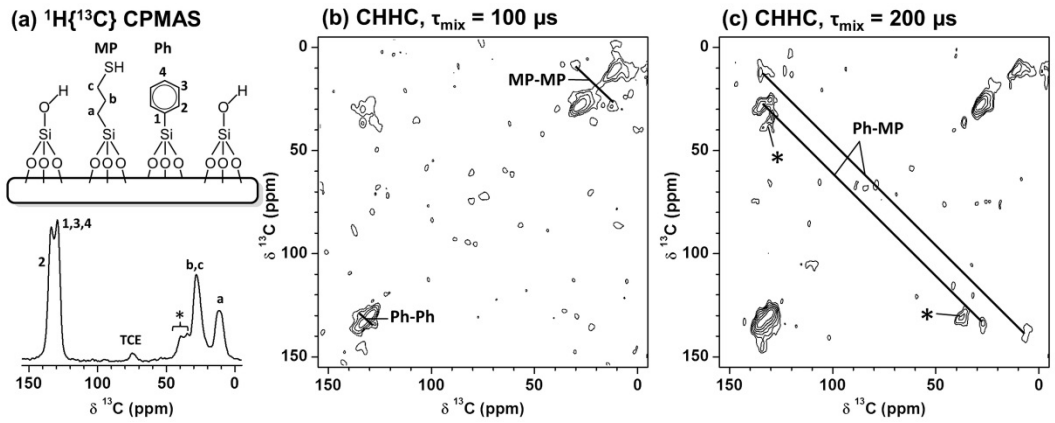

Figure 4 DNP-enhanced 1D $^{13}C\{^1H\}$ CPMAS (a) and 2D ^{13}C-^{13}C homonuclear correlation (b, c) spectra of bifunctionalized mesoporous silica nanoparticles obtained with ν_R = 9.5 kHz, τ_{CP} = 2 ms and τ_{RD} = 7 s. Spectrum (a) was acquired in just 14 s (2 scans); spectrum b was obtained with τ_{CP2} = 2 ms, τ_{mix} = 100 μs and 200 μs, 40 t_1 steps with Δt_1 = 50 μs, 80 scans per row, and AT = 12.5 h. Asterisks denote spinning sidebands.

4. Conclusion

In summary, we have demonstrated a DNP-based approach for observing intermolecular ^{13}C-^{13}C homonuclear correlations at natural abundance in complex samples. Most notably, the use of the CHHC technique improved the sensitivity and allowed the successful detection of intermolecular correlations on a catalyst surface. In addition, the large ^{1}H spin bath provided by the solvent expedited the $^{13}C \rightarrow {}^{1}H$ magnetization transfer during the second cross-polarization and suppressed the intensity of diagonal signals. Since the CHHC scheme does not suffer from the dipolar truncation and relaxation losses found in the DQ recoupling techniques, isotopic labelling will further improve the sensitivity of longer-range correlations. This approach can also be implemented in other homonuclear and heteronuclear experiments, such as SiHHSi and CHHN.

ASSOCIATED CONTENT

Supporting Information. Supporting Information is available free of charge on the ACS Publication website at DOI. The SI contains: ^{13}C-^{13}C SQ/SQ correlation spectrum of polyacrylamide obtained using DARR recoupling, ^{13}C-^{13}C SQ/SQ correlation spectra of semicrystalline cellulose obtained using CHHC scheme with various contact time, slice of ^{13}C-^{13}C homonuclear correlation spectrum of semicrystalline cellulose obtained by CHHC scheme.

Notes

The authors declare no competing financial interests.

ACKNOWLEDGMENT

The authors thank Dr. F. A. Perras for helpful discussions. This research is supported by the U.S. Department of Energy, Office of Basic Energy Sciences, Division of Chemical Sciences, Geosciences, and Biosciences through the Ames Laboratory. The Ames Laboratory is operated for the U.S. Department of Energy by Iowa State University under Contract No. DE-AC02-07CH11358.

REFERENCES

(1) Brown, S. P. Applications of High-Resolution H-1 Solid-State NMR. *Solid State Nucl. Magn. Reson.* **2012**, *41*, 1-27.

(2) Kobayashi, T.; Mao, K.; Paluch, P.; Nowak-Krol, A.; Sniechowska, J.; Nishiyama, Y.; Gryko, D. T.; Potrzebowski, M. J.; Pruski, M. Study of Intermolecular Interactions in the Corrole Matrix by Solid-State NMR under 100 kHz MAS and Theoretical Calculations. *Angew. Chem. Int. Ed.* **2013**, *52*, 14108-14111.

(3) Maly, T.; Debelouchina, G. T.; Bajaj, V. S.; Hu, K.-N.; Joo, C.-G.; Mak-Jurkauskas, M. L.; Sirigiri, J. R.; van der Wel, P. C. A.; Herzfeld, J.; Temkin, R. J., et al. Dynamic Nuclear Polarization at High Magnetic Fields. *J. Chem. Phys.* **2008**, *128*.

(4) Becerra, L. R.; Gerfen, G. J.; Bellew, B. F.; Bryant, J. A.; Hall, D. A.; Inati, S. J.; Weber, R. T.; Un, S.; Prisner, T. F.; McDermott, A. E., et al. A Spectrometer for Dynamic Nuclear-Polarization and Electron-Paramagnetic-Resonance at High-Frequencies. *J. Magn. Reson. Ser. A* **1995**, *117*, 28-40.

(5) Rosay, M.; Lansing, J. C.; Haddad, K. C.; Bachovchin, W. W.; Herzfeld, J.; Temkin, R. J.; Griffin, R. G. High-frequency Dynamic Nuclear Polarization in MAS Spectra of Membrane and Soluble Proteins. *J. Am. Chem. Soc.* **2003**, *125*, 13626-13627.

(6) Sauvée, C.; Rosay, M.; Casano, G.; Aussenac, F.; Weber, R. T.; Ouari, O.; Tordo, P. Highly Efficient, Water-Soluble Polarizing Agents for Dynamic Nuclear Polarization at High Frequency. *Angew. Chem. Int. Ed.* **2013**, *52*, 10858-10861.

(7) Zagdoun, A.; Casano, G.; Ouari, O.; Schwarzwälder, M.; Rossini, A. J.; Aussenac, F.; Yulikov, M.; Jeschke, G.; Copéret, C.; Lesage, A., et al. Large Molecular Weight Nitroxide

Biradicals Providing Efficient Dynamic Nuclear Polarization at Temperatures up to 200 K. *J. Am. Chem. Soc.* **2013**, *135*, 12790-12797.

(8) Takahashi, H.; Lee, D.; Dubois, L.; Bardet, M.; Hediger, S.; De Paepe, G. Rapid Natural-Abundance 2D C-13-C-13 Correlation Spectroscopy Using Dynamic Nuclear Polarization Enhanced Solid-State NMR and Matrix-Free Sample Preparation. *Angew. Chem. Int. Ed.* **2012**, *51*, 11766-11769.

(9) Rossini, A. J.; Zagdoun, A.; Hegner, F.; Schwarzwalder, M.; Gajan, D.; Coperet, C.; Lesage, A.; Emsley, L. Dynamic Nuclear Polarization NMR Spectroscopy of Microcrystalline Solids. *J. Am. Chem. Soc.* **2012**, *134*, 16899-16908.

(10) Rossini, A. J.; Widdifield, C. M.; Zagdoun, A.; Lelli, M.; Schwarzwalder, M.; Coperet, C.; Lesage, A.; Emsley, L. Dynamic Nuclear Polarization Enhanced NMR Spectroscopy for Pharmaceutical Formulations. *J. Am. Chem. Soc.* **2014**, *136*, 2324-2334.

(11) Lee, D.; Monin, G.; Duong, N. T.; Lopez, I. Z.; Bardet, M.; Mareau, V.; Gonon, L.; De Paëpe, G. Untangling the Condensation Network of Organosiloxanes on Nanoparticles using 2D Si-29-Si-29 Solid-State NMR Enhanced by Dynamic Nuclear Polarization. *J. Am. Chem. Soc.* **2014**, *136*, 13781-13788.

(12) Mollica, G.; Dekhil, M.; Ziarelli, F.; Thureau, P.; Viel, S. Quantitative Structural Constraints for Organic Powders at Natural Isotopic Abundance Using Dynamic Nuclear Polarization Solid-State NMR Spectroscopy. *Angew. Chem. Int. Ed.* **2015**, *54*, 6028-6031.

(13) Marker, K.; Pingret, M.; Mouesca, J. M.; Gasparutto, D.; Hediger, S.; De Paepe, G. A New Tool for NMR Crystallography: Complete C-13/N-15 Assignment of Organic Molecules at Natural Isotopic Abundance Using DNP-Enhanced Solid-State NMR. *J. Am. Chem. Soc.* **2015**, *137*, 13796-13799.

(14) Perras, F. A.; Luo, H.; Zhang, X. M.; Mosier, N. S.; Pruski, M.; Abu-Omar, M. M. Atomic-Level Structure Characterization of Biomass Pre- and Post-Lignin Treatment by Dynamic Nuclear Polarization-Enhanced Solid-State NMR. *J. Phys. Chem. A* **2017**, *121*, 623-630.

(15) Marker, K.; Paul, S.; Fernandez-de-Alba, C.; Lee, D.; Mouesca, J. M.; Hediger, S.; De Paepe, G. Welcoming Natural Isotopic Abundance in Solid-State NMR: Probing pi-Stacking and Supramolecular Structure of Organic Nanoassemblies Using DNP. *Chem. Sci.* **2017**, *8*, 974-987.

(16) Mouat, A. R.; Kobayashi, T.; Pruski, M.; Marks, T. J.; Stair, P. Direct Spectroscopic Evidence for Isolated Silanols in SiO_x/Al_2O_3 and their Formation Mechanism in Atomic Layer Deposition. *J. Chem. Phys. C, J. Chem. Phys. C*, **2017**, *121*, 6060-6064.

(17) Kobayashi, T.; Singappuli-Arachchige, D.; Wang, Z.; Slowing, I. I.; Pruski, M. Spatial Distribution of Organic Functional Groups Supported on Mesoporous Silica Nanoparticles: A Study by Conventional and DNP-Enhanced Si-29 Solid-State NMR. *Phys. Chem. Chem. Phys.* **2017**, *19*, 1781-1789.

(18) Hohwy, M.; Jakobsen, H. J.; Eden, M.; Levitt, M. H.; Nielsen, N. C. Broadband Dipolar Recoupling in the Nuclear Magnetic Resonance of Rotating Solids: A Compensated C7 Pulse Sequence. *J. Chem. Phys.* **1998**, *108*, 2686-2694.

(19) Bax, A.; Freeman, R. Investigation of Complex Networks of Spin-Spin Coupling by Two-Dimensional NMR. *J. Magn. Reson.* **1981**, *44*, 542-561.

(20) Szeverenyi, N. M.; Sullivan, M. J.; Maciel, G. E. Observation of Spin Exchange by Two-Dimensional Fourier-Transform C-13 Cross Polarization-Magic-Angle Spinning. *J. Magn. Reson.* **1982**, *47*, 462-475.

(21) Takegoshi, K.; Nakamura, S.; Terao, T. C-13-H-1 Dipolar-Assisted Rotational Resonance in Magic-angle Spinning NMR. *Chem. Phys. Lett.* **2001**, *344*, 631-637.

(22) Morcombe, C. R.; Gaponenko, V.; Byrd, R. A.; Zilm, K. W. Diluting abundant Spins by Isotope Edited Radio Frequency Field Assisted Diffusion. *J. Am. Chem. Soc.* **2004**, *126*, 7196-7197.

(23) Weingarth, M.; Demco, D. E.; Bodenhausen, G.; Tekely, P. Improved Magnetization Transfer in Solid-state NMR with Fast Magic Angle Spinning. *Chem. Phys. Lett.* **2009**, *469*, 342-348.

(24) Wilhelm, M.; Feng, H.; Tracht, U.; Spiess, H. W. 2D CP/MAS C-13 Isotropic Chemical Shift Correlation Established by H-1 Spin Diffusion. *J. Magn. Reson.* **1998**, *134*, 255-260.

(25) Mulder, F. M.; Heinen, W.; van Duin, M.; Lugtenburg, J.; de Groot, H. J. M. Spin Diffusion with C-13 Selection and Detection for the Characterization of Morphology in Labeled Polymer Blends with MAS NMR. *J. Am. Chem. Soc.* **1998**, *120*, 12891-12894.

(26) de Boer, I.; Bosman, L.; Raap, J.; Oschkinat, H.; de Groot, H. J. M. 2D(13)C-C-13 MAS NMR Correlation Spectroscopy with Mixing by True H-1 Spin Diffusion Reveals Long-

Range Intermolecular Distance Restraints in Ultra High Magnetic Field. *J. Magn. Reson.* **2002**, *157*, 286-291.

(27) Lange, A.; Luca, S.; Baldus, M. Structural Constraints from Proton-Mediated Rare-Spin Correlation Spectroscopy in Rotating Solids. *J. Am. Chem. Soc.* **2002**, *124*, 9704-9705.

(28) Aluas, M.; Tripon, C.; Griffin, J. M.; Filip, X.; Ladizhansky, V.; Griffin, R. G.; Brown, S. P.; Filip, C. CHHC and H-1-H-1 magnetization exchange: Analysis by Experimental Solid-State NMR and 11-Spin Density-Matrix Simulations. *J. Magn. Reson.* **2009**, *199*, 173-187.

(29) Nishiyama, Y.; Langan, P.; Chanzy, H. Crystal Structure and Hydrogen-Bonding System in Cellulose 1 Beta from Synchrotron X-Ray and Neutron Fiber Diffraction. *J. Am. Chem. Soc.* **2002**, *124*, 9074-9082.

(30) Chen, Q.; Schmidt-Rohr, K. Measurement of the Local H-1 Spin-Diffusion Coefficient in Polymers. *Solid State Nucl. Magn. Reson.* **2006**, *29*, 142-152.

TOC GRAPHIC